Supporting Information

Carbonyl-Linked Cobalt Polyphthalocyanines as High-Selectivity Catalyst for Electrochemical CO_2 Reduction

Haisen Jin‡[a,b], *Yajing Di*‡[a,b], *Yueang Gu*[a,b], *Yu Chen*[a,b], *Meiling Dou*[a,b], *Zhengping Zhang* *[a,b], *Feng Wang* *[a,b]

a State Key Laboratory of Chemical Resource Engineering, Beijing Key Laboratory of Electrochemical Process and Technology for Materials, Beijing University of Chemical Technology, Beijing 100029, P R China.

b Beijing Advanced Innovation Center for Soft Matter Science and Engineering, Beijing University of Chemical Technology, Beijing 100029, P. R. China.

* Corresponding email: zhangzhengping@mail.buct.edu.cn (Z. Zhang);
wangf@mail.buct.edu.cn (F. Wang)

‡ These authors contributed equally to this work.

Chemicals.

Cobalt chloride hexahydrate [$CoCl_2 \cdot 6H_2O$, Aladdin, CAS#: 7791-13-1], phthalic anhydride (PA) [$C_8H_4O_3$, Sinopharm, CAS#: 85-44-9], pyromellitic dianhydride (PMDA) [$C_{10}H_2O_6$, Aladdin, CAS#: 89-32-7], 3,3',4,4'-benzophenonetetracarboxylicdianhydride (BTDA) [$C_{17}H_6O_7$, Sinopharm, CAS#: 2421-28-5], urea [$(NH_2)_2CO$, Aladdin, CAS#: 57-13-6], ammonium chloride [NH_4Cl, Aladdin, CAS#: 12125-02-9], ammonium molybdate tetrahydrate [$(NH_4)_6Mo_7O_{24} \cdot 4H_2O$, Sinopharm, CAS#: 12054-85-2], potassium bicarbonate [$KHCO_3$, Aladdin, CAS#: 298-14-6], and Nafion [5%, DuPont] were used without further purification. High purity carbon dioxide and nitrogen gas were bought from Beijing AP BAIF Gases Industry Co. Ltd.

Preparations

The carbonyl-linked cobalt polyphthalocyanines (CL-CoPPc) were prepared by a solid phase synthesis method in a muffle furnace. 3,3',4,4'-benzophenonetetracarboxylicdianhydride (BTDA) (0.155 g), $CoCl_2 \cdot 6H_2O$ (0.08 g), urea (0.3 g), NH_4Cl (0.045 g), and $(NH_4)_6Mo_7O_{24} \cdot 4H_2O$ (0.015 g) were ground together, and then transferred into a 50 mL crucible. The mixture was heated at 140 °C for 1 hour, and subsequently heated up to 240 °C for another 3 hours. After cooling to room temperature, the obtained solid was washed with water, acetone, and ethanol. The final product was dried under vacuum at 80 °C for 24 hours. The cobalt polyphthalocyanines (CoPPc) and cobalt phthalocyanine (CoPc) were synthesized in the similar route by using pyromellitic dianhydride (0.105 g) and phthalic anhydride (0.143

g) to replace 3,3',4,4'-benzophenonetetracarboxylic dianhydride, respectively.

The preparation of CL-CoPPc/CNT was similar to the synthesis of CL-CoPPc. $CoCl_2 \cdot 6H_2O$ (0.08 g), deionized water (5 mL) and a certain amount of purified MWCNTs were mixed and adequately stirred, then dried under vacuum at 80 °C overnight. After completely drying, the premixed material, BTDA (0.155 g), urea (0.3 g), NH_4Cl (0.045 g) and $(NH_4)_6Mo_7O_{24} \cdot 4H_2O$ (0.015 g) were ground together, and then transferred into a 50 mL crucible. The mixture was heated at 140 °C for 1 hour, and subsequently heated up to 240 °C for another 3 hours. After cooling to room temperature, the obtained solid was washed with water, acetone, and ethanol. The final product was dried under vacuum at 80 °C for 24 hours. Depending on the amount of MWCNTs (1.262 g, 0.56 g, 0.327 g, 0.21 g), CL-CoPPc/CNT with phthalocyanine content of 10 wt%, 20 wt%, 30 wt% and 40 wt% were obtained respectively. CNT-supported cobalt phthalocyanine (CoPc/CNT) and CNT-supported cobalt polyphthalocyanine (CoPPc/CNT) were synthesized in the similar route by using pyromellitic dianhydride (0.105 g) and phthalic anhydride (0.143 g) to replace BTDA, respectively.

Characterization

Field-emission scanning electron microscopy (FE-SEM, JSM-6701/JEOL), transmission electron microscopy (TEM, JEOL JEM-2100) and aberration-corrected scanning transmission electron microscope (STEM, JEMARM200F/JEOL) equipped with a spherical aberration corrector were used to observe the morphologic and structural characteristics of the samples. The Fourier Transform InfraRed (FT-IR) analysis was performed on a Nicolet 8700/Continuum

XL with wavenumber from 2300 to 500 cm^{-1}. The ultraviolet-visible (UV-vis) absorption spectroscopy was carried out on a Shimadzu UV-2450 with wavelength from 300 to 900 nm. Raman spectra were record on a Horiba Jobin Yvon LabRam HR800 with an excitation wavelength of 633 nm. Solid-state nuclear magnetic resonance (NMR) spectra were measured on a Bruker AVANCE III 600M spectrometer operating at 75.5 MHz for ^{13}C. The X-ray diffraction profile (XRD) was obtained on a Rigaku D/Max 2500 VB2+/PC diffractometer with Cu Ka radiation (λ=1.54056 Å) as the X-ray source. The elemental oxidation states of the samples were investigated by X-ray photoelectron spectrum (XPS, Thermo Fisher Scientific ESCALAB 250). The elemental spectra were all corrected with respect to C1s peaks at 284.6 eV. The thermogravimetric analysis (TGA) was obtained on a Rigaku TG-8120 with under the atmosphere of air at a heating rate of 5 K min^{-1}.

Electrode preparation and electrochemical measurements

The catalyst ink in H-cell was prepared as follows. 4 mg of catalyst and 20 μL of 5 wt% Nafion solution were dispersed in 2 ml ethanol assisted with ultrasonication for 0.5 h. Then 10 μL catalyst ink was drop cast onto glassy carbon electrode (composite catalyst loading: 0.16 mg cm^{-2}) as the working electrode. The electrochemistry tests were carried out in a two-compartment electrochemical cell (Scheme S1) with a three-electrode system. The saturated Ag/AgCl electrode was the reference electrode, while a Pt gauze was used as the counter electrode. the electrolyte was saturated with either CO_2 or N_2. Electrocatalytic reduction of CO_2 was carried out in CO_2-saturated 0.5 M $KHCO_3$ solution (pH 7.2) at room temperature and

under atmospheric pressure. During the ECR measurements, the electrolyte in the cathodic compartment was stirred at a speed of 400 rpm. All potentials were converted to RHE scale based on the Nernst equation.

For the ECR measurements based on GDE, 25 mg of composite catalyst and 55 μL of 5 wt% Nafion solution were dispersed in 10 mL ethanol, then the mixture was vigorously sonicated for 30 min to form a uniform ink. The ink was sprayed onto a 2×2 cm^2 carbon fiber paper (SGL28BC) with a size of 2.5×2.5 cm^2. The composite catalyst loading was achieved to be 3 mg cm^{-2}. Electrochemical tests were carried out in a flow cell (Scheme S2), the electrolyte was 0.5 M $KHCO_3$ (pH 7.2), and the flow rate was 20 sccm by peristaltic pumps. During chronopotentiometry tests, high-purity CO_2 gas was delivered into the cathodic compartment at a flow rate of 20 sccm. The gas products were analyzed by gas chromatograph (Shimazu GC2030) and the Faradaic efficiency was calculated as follows:

$$FE\,(\%) = \frac{C \times 10^{-6} \times V \times 10^{-3} \times F \times n}{22.4 \times I \times t}$$

Where C (ppm) is the product concentration, V is the flow rate of CO_2 (20 mL min^{-1}), F is the Faraday constant (96485 C mol^{-1}), n (=2) is the number of electrons required to form a molecule of CO or H_2, and I (A) is the current. In this experiment, since the reaction area is 1 cm^2, I is numerically equal to the current density of the reaction. t (=60 s) is the time.

The CO mass activity (mA mg^{-1}) is calculated by the following equation:

$$j_{CO}^{m} = \frac{j \times FE_{CO}}{w}$$

where j (mA cm^{-2}) is the current density measured by potentiostatic testing, FEco is the CO Faradaic efficiency, and w (mg cm^{-2}) is the catalyst metal loading measured by thermogravimetry.

TOF is calculated as the following:

$$TOF = \frac{TOF_0}{f} = \frac{j_{tot} \times FE_{CO}}{2F \times n_{tot} \times f}$$

Where j_{tot} is the total reduction current, *FE*co is CO Faradic efficiency, *F* is the Faraday constant (96485 C mol^{-1}). n_{tot} is the total amount of Co on the working electrode.

f is the surface fraction of electrochemically active Co sites and calculated as following:

$$f = \frac{n}{n_{tot}} = \frac{M\int UI}{mwvF}$$

Where *n* is the amount of surface active Co on the working electrode, M is the atomic weight of Co (58.93 g/mol), *U* is Co^{II}/Co^{I} redox region potential (V), *I* is Co^{II}/Co^{I} redox region current (mA), m is the mass of the electrocatalyst loaded on the working electrode, w is the weight fraction of Co in the electrocatalyst determined from the thermogravimetry. *v* is Co^{II}/Co^{I} redox region scanning rate (V/s).

σ_H is calculated as the following:

$$\sigma_H = \frac{t}{RS}$$

Where σ_H, t, R, S represent proton conductivity (S cm^{-1}), thickness of catalysts (cm), resistance (Ω) and contact area (cm^2).

the activation energy is calculated as the following:

$$Ln(\sigma_H T) = LnA - \frac{E_a}{K_B T}$$

Where T, E_a, k_B, A represent temperature (K), activation energy (eV), Boltzmann's constant (1.38×10^{-23} J K^{-1}) and preexponential factor.

Results and discussion

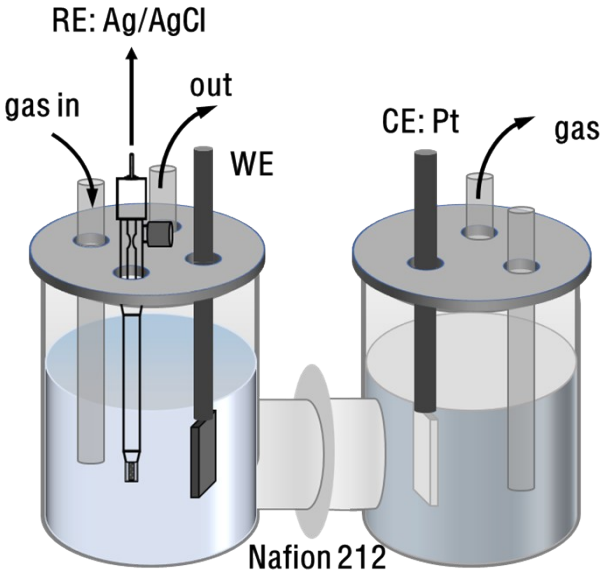

Scheme S1. Illustration of the H-cell.

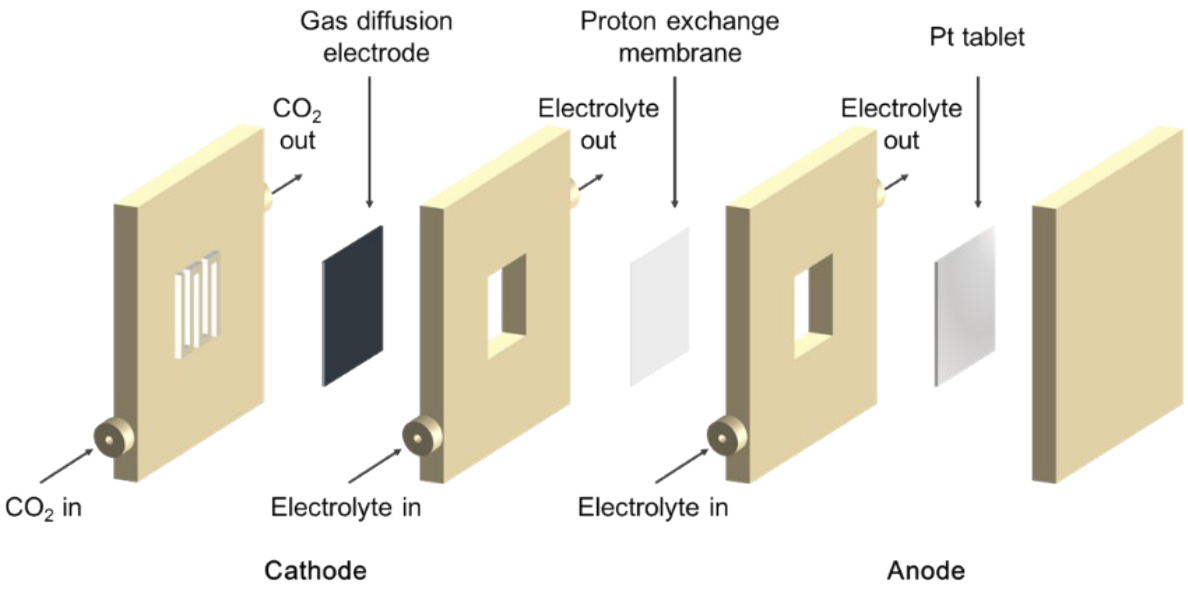

Scheme S2. Illustration of the flow cell.

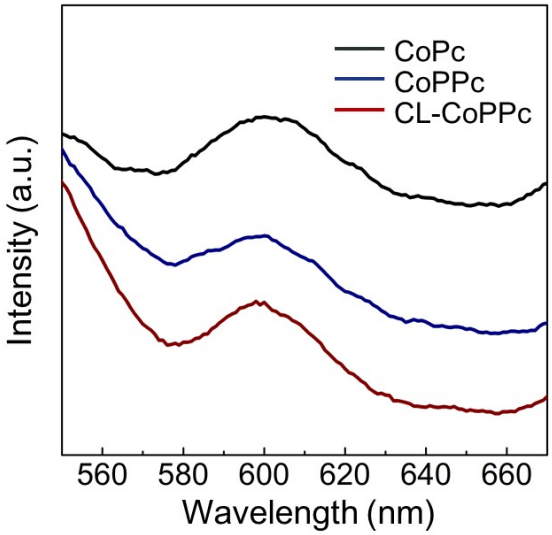

Figure S1. Fluorescence spectra of CoPc, CoPPc and CL-CoPPc.

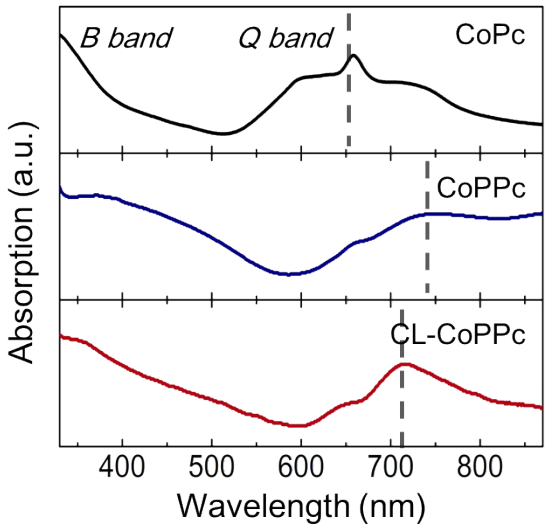

Figure S2. Ultraviolet-visible spectra of CoPc, CoPPc and CL-CoPPc.

In ultraviolet-visible spectra, two characteristic absorbance bands of phthalocyanine were observed at 550-800 nm (*Q* band) and 300-450 nm (*B* band) as the results of $a_{1u}(\pi)$-$e_g(\pi^*)$ and $a_{2u}(\pi)$-$e_g(\pi^*)$ transition from the highest occupied molecular orbital (HOMO) to the lowest unoccupied molecular orbital (LUMO), respectively.[1]

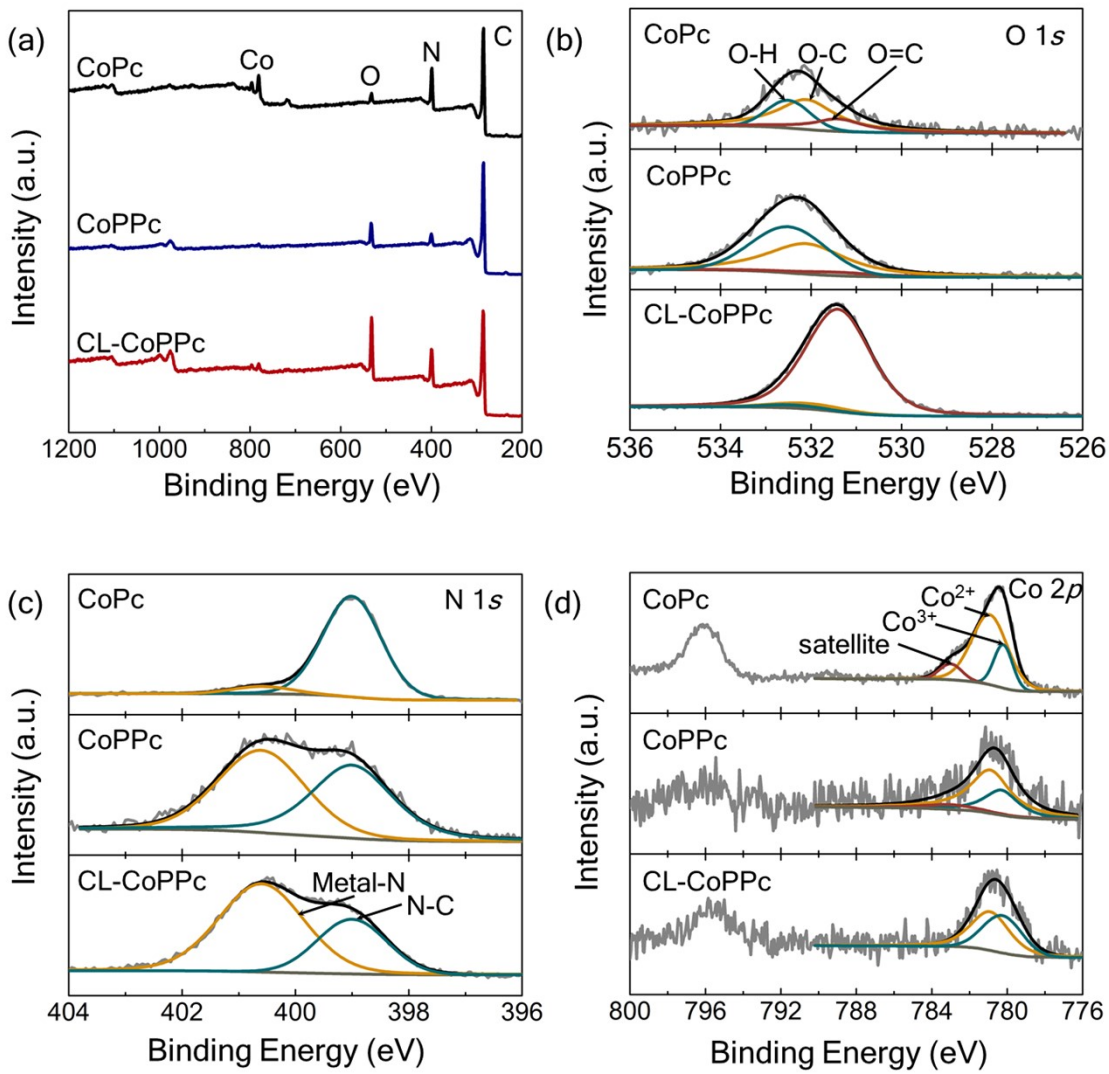

Figure S3. a) The XPS survey spectra of CoPc, CoPPc and CL-CoPPc. The high-resolution XPS spectra of b) O 1*s*, c) N 1*s*, d) Co 2*p*, for CoPc, CoPPc and CL-CoPPc.

The high-resolution spectra of Co 2*p* for all materials could be deconvoluted into Co^{3+} (780.2 eV), Co^{2+} (780.9 eV), and satellite (783.0 eV). The N 1*s* binding energy at 400.6 eV is related to four central nitrogen atoms located in red dash circle, noted as Metal−N. Another N 1*s* position at 399.0 eV corresponds to other four aza-bridging nitrogen atoms located in green dash circle, noted as N-C. The XPS spectrum of N 1*s* for CL-CoPPc was similar to CoPPc, indicating CL-CoPPc also had phthalocyanine-based conjugated polymer network structure. The pass energy is 200 eV for survey, and 30 eV for high resolution scans, the same below.

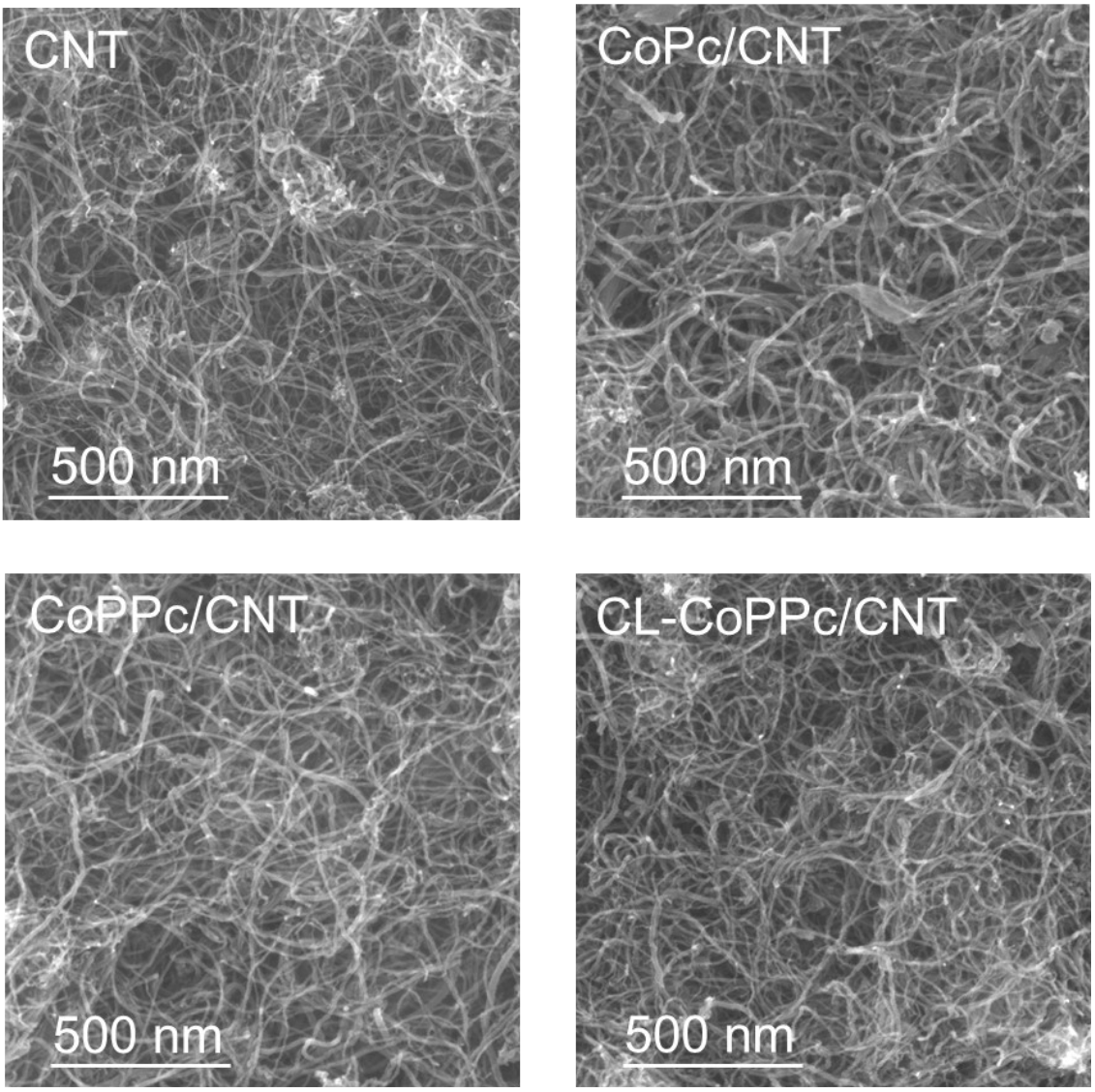

Figure S4. SEM images of carbon nanotubes (CNT), carbon nanotubes supported CoPc (CoPc/CNT), CoPPc (CoPPc/CNT), and CL-CoPPc (CL-CoPPc/CNT).

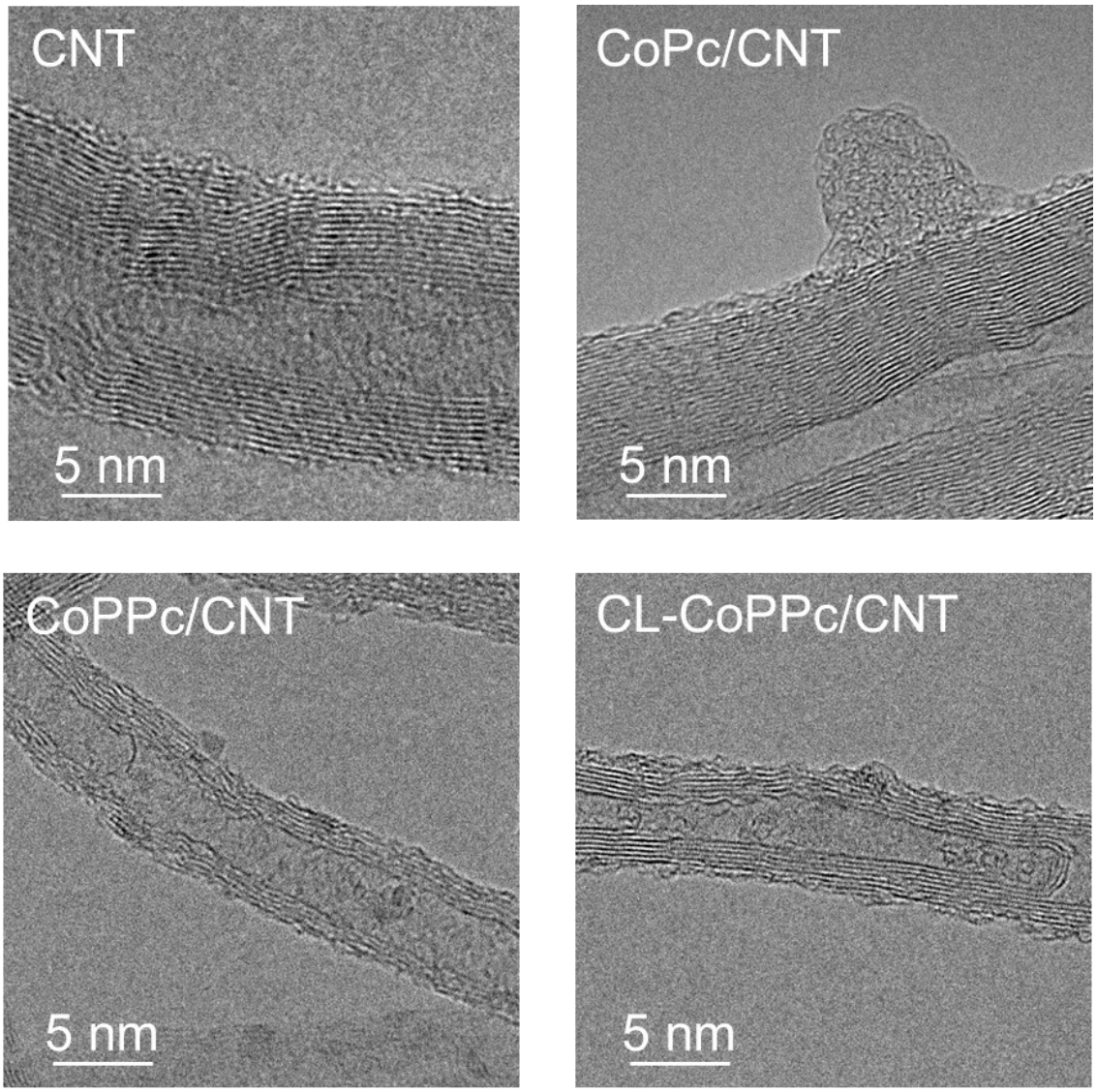

Figure S5. TEM images of CNT, CoPc/CNT, CoPPc/CNT and CL-CoPPc/CNT.

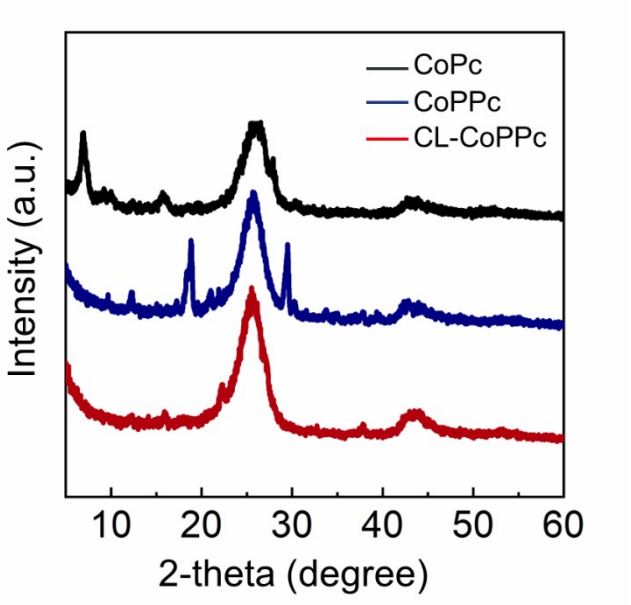

Figure S6. XRD patterns of CoPc, CoPPc and CL-CoPPc.

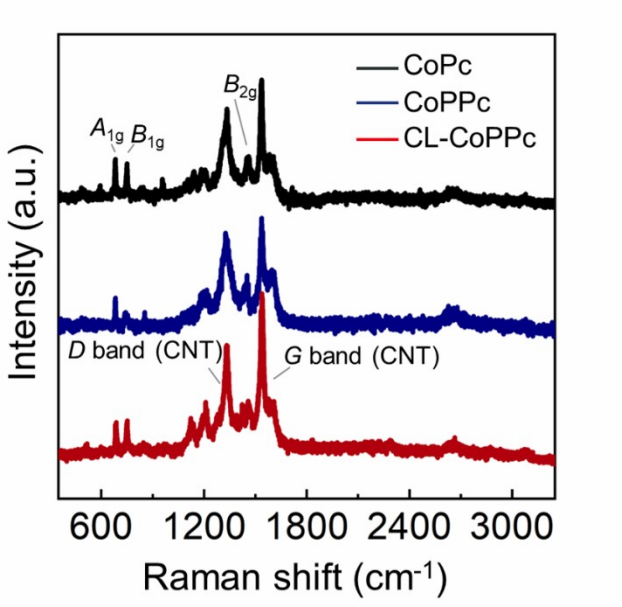

Figure S7. Raman spectra of CoPc, CoPPc and CL-CoPPc.

After the heterogenization with nanocarbons, Raman spectra show the apparent characteristic peaks corresponding to phthalocyanines macrocycles in the CL-CoPPc, CoPPc and CoPc samples. However, CL-CoPPc did not exhibits crystallization peaks in XRD patterns (Figure S6), which was different from CoPPc and CoPc. It indicated that the carbonyl linkages could reduce the π-π stacking induced crystallization.

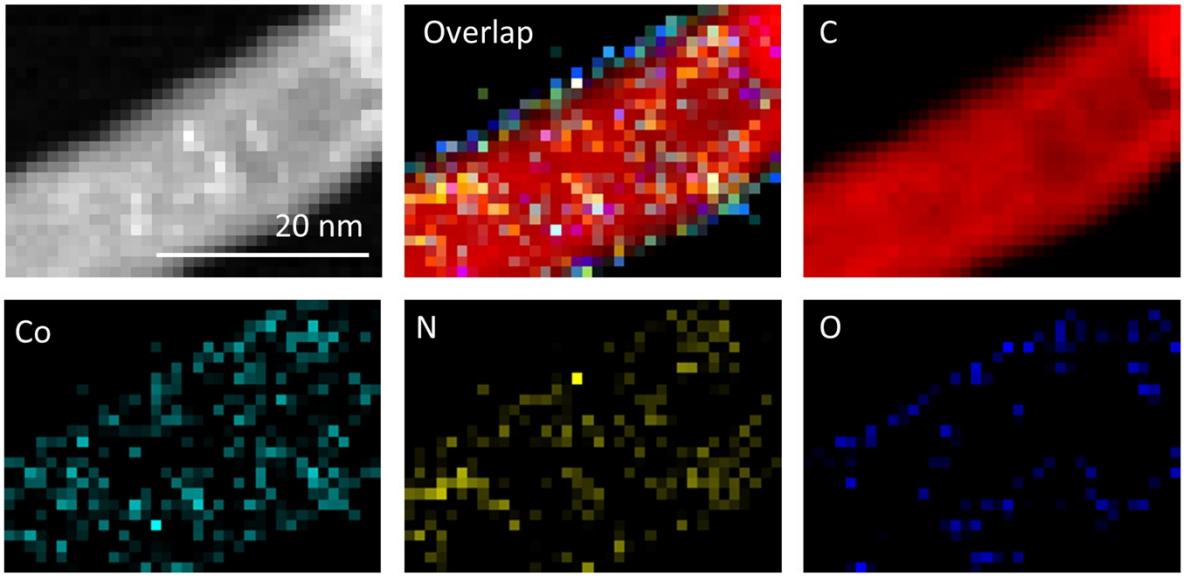

Figure S8. STEM-EELS elemental mapping images of CNT supported CL-CoPPc

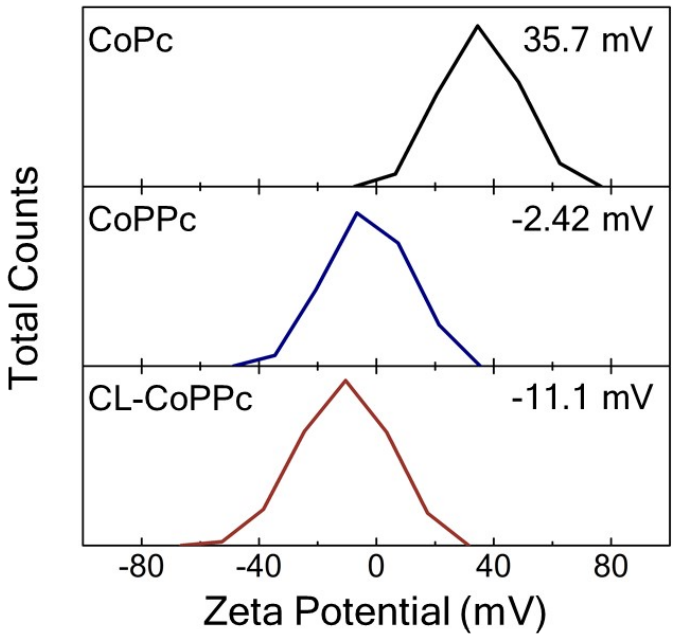

Figure S9. Zeta-potentials of CNT supported CoPc, CoPPc, and CL-CoPPc.

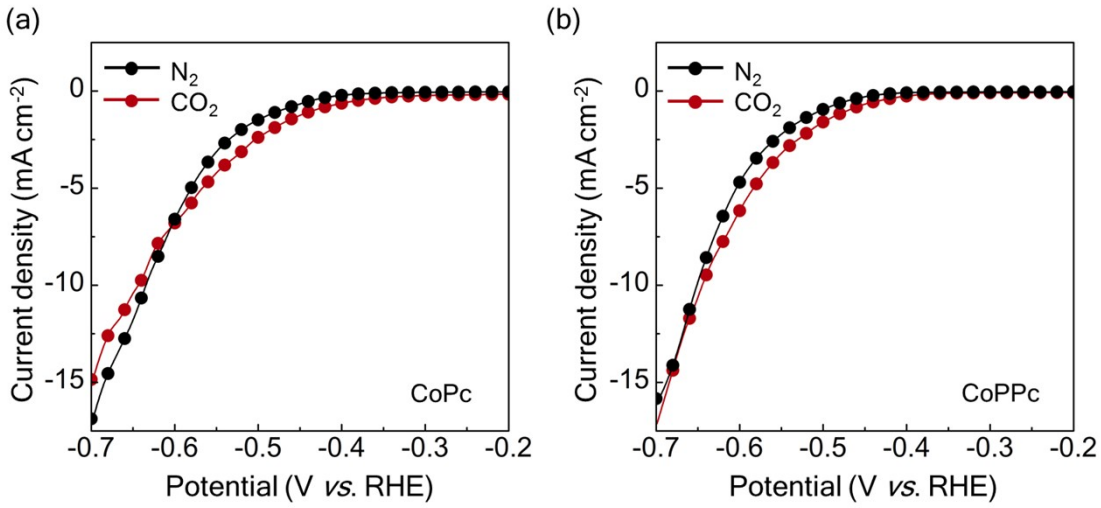

Figure S10. The LSV curves of a) CoPc/CNT and b) CoPPc/CNT on glassy carbon electrode. The scan rate is 10 mV/s, the same below.

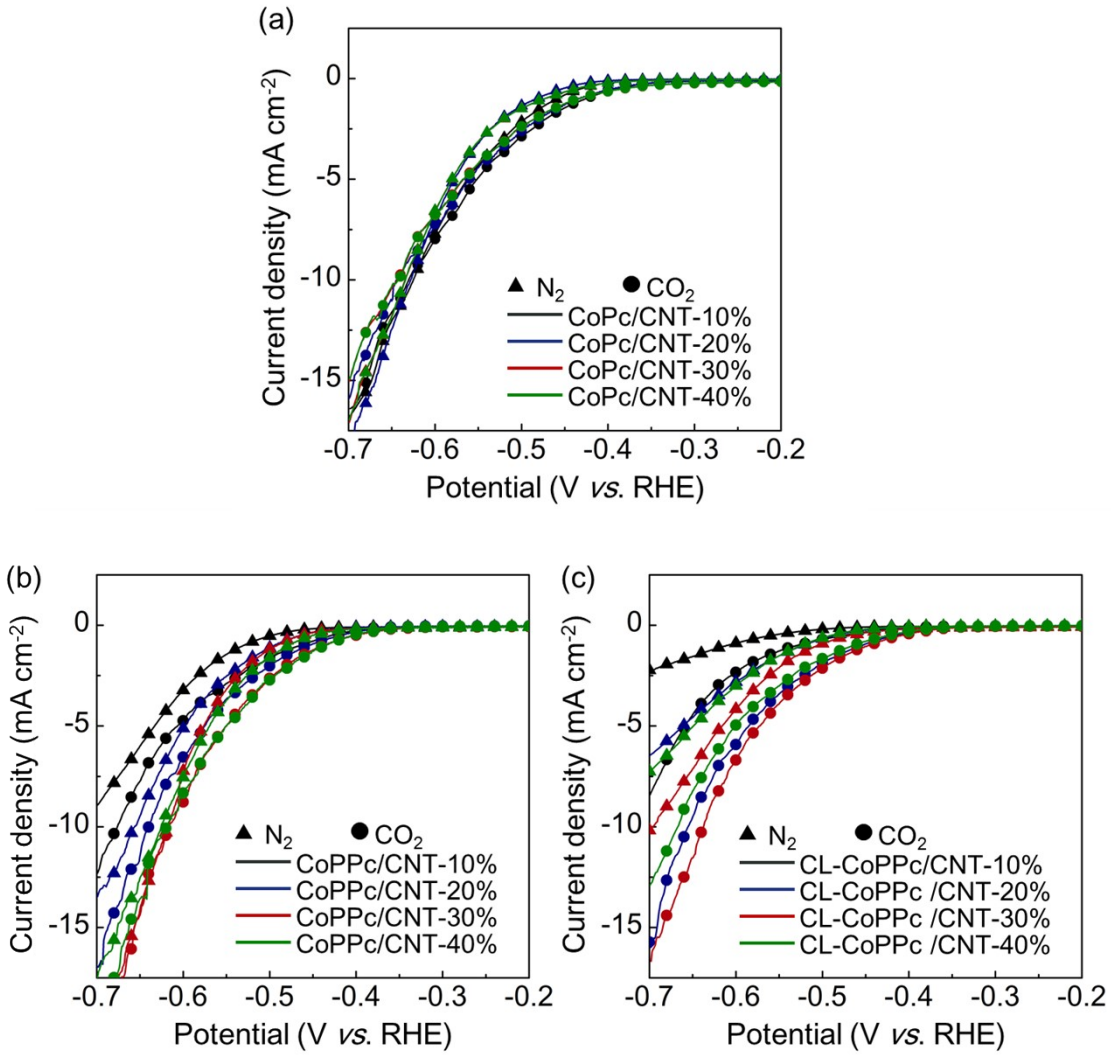

Figure S11. LSV curves of a) CoPc/CNT, b) CoPPc/CNT and c) CL-CoPPc/CNT with different contents on glassy carbon electrode.

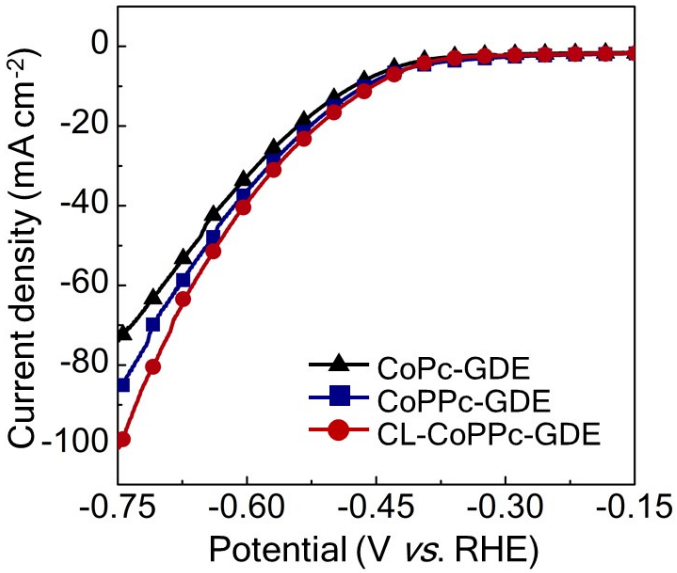

Figure S12. LSV curves of CoPc, CoPPc and CL-CoPPc on gas diffusion electrode.

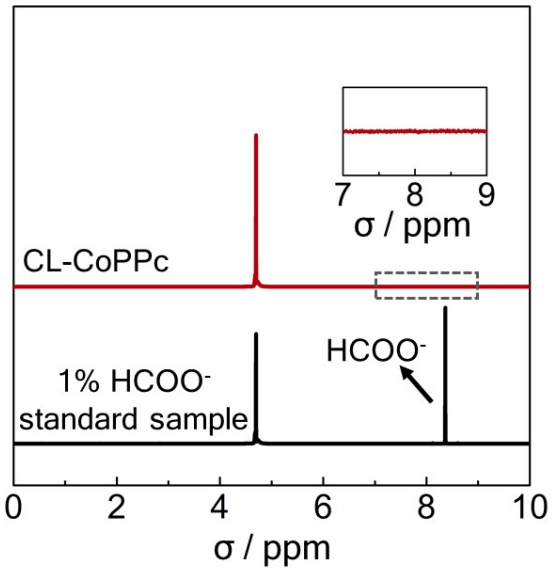

Figure S13. ^{1}H-NMR of liquid product from CL-CoPPc and the standard $HCOO^{-}$ sample.

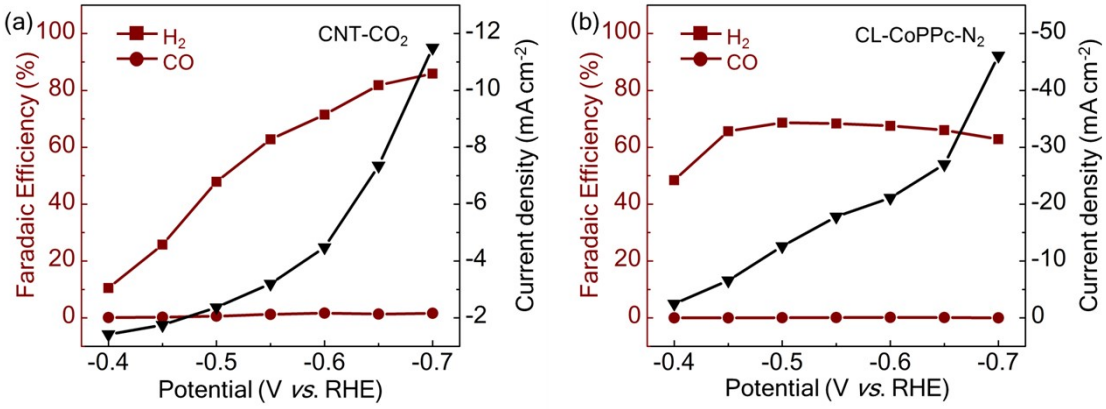

Figure S14. ECR performance of (a) CNTs in CO_2 atmosphere and (b) CL-CoPPc in N_2 atmosphere.

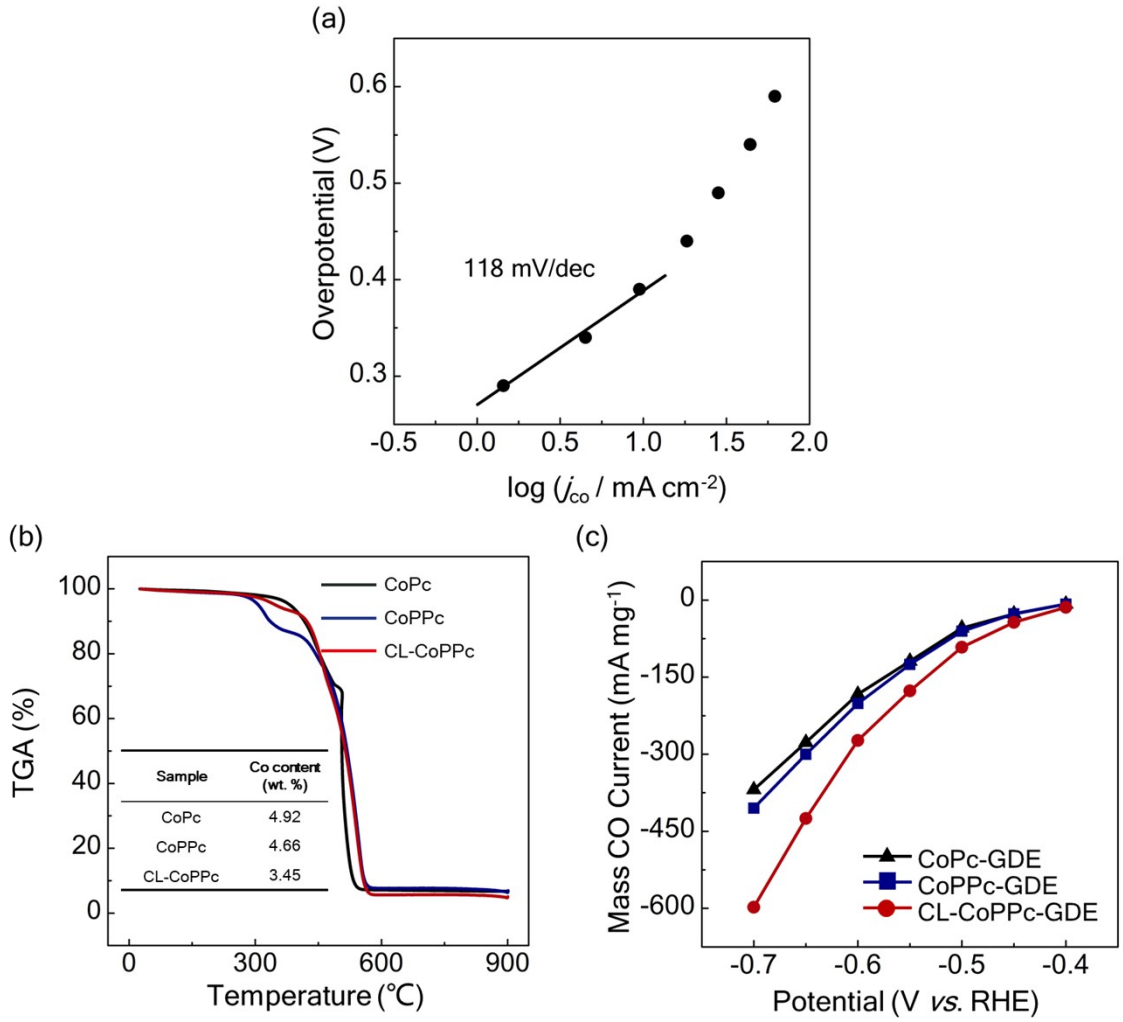

Figure S15. (a) Tafel slope of CL-CoPPc modified GDE. (b) Thermogravimetric analysis (TGA) of CNT supported CoPc, CoPPc, and CL-CoPPc. Inset: the metal Co content derived from TGA results. (c) Mass CO Current of CoPc, CoPPc, and CL-CoPPc modified GDEs derived from TGA results.

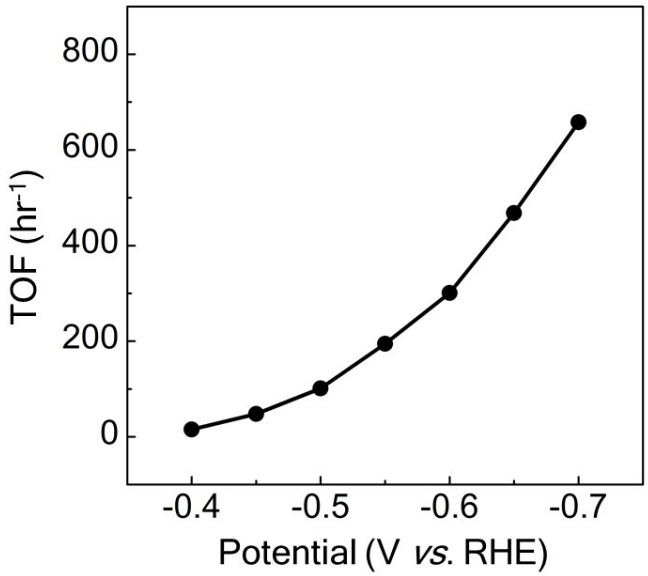

Figure S16. TOF of the CL-CoPPc (assumed all the atomic cobalt sites participate in the ECR process).

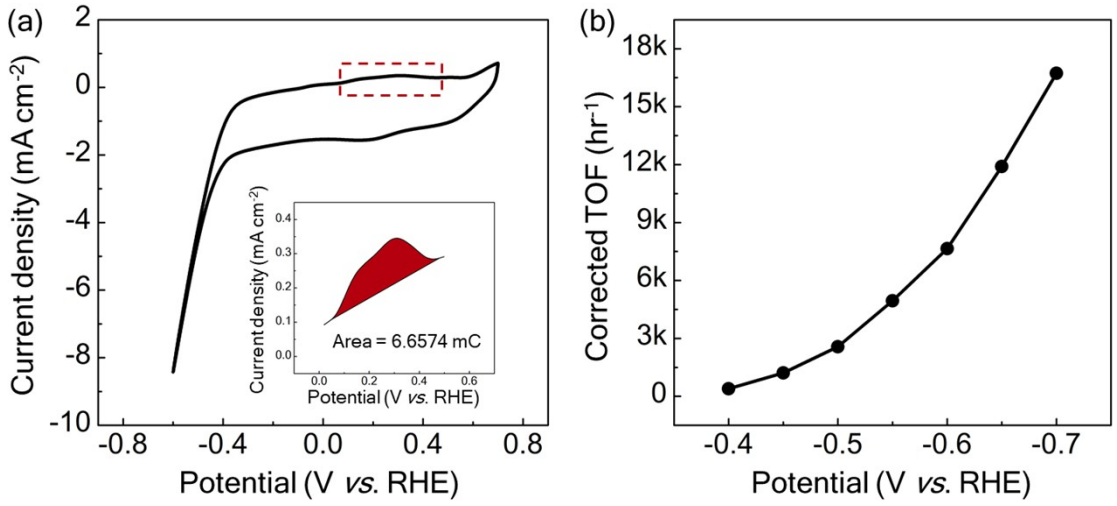

Figure S17. (a) CV curve of the CL-CoPPc/CNT in N_2-saturated 0.5 M $KHCO_3$ (pH = 8.4). Inset shows the total charge integrated from the Co^{I}/Co^{II} anodic wave. (b) TOF of the CL-CoPPc/CNT (assumed all the atomic cobalt sites participate in the ECR process).

We integrated the anodic wave in the CV curve of CL-CoPPc/CNT and then calculated the amount of surface-active Co by assuming a one-electron redox process:

$$n_{act} = \frac{Q}{F} = \frac{6.6574 \times 10^{-3}\ C}{96485\ C/mol} = 6.90 \times 10^{-8}\ mol$$

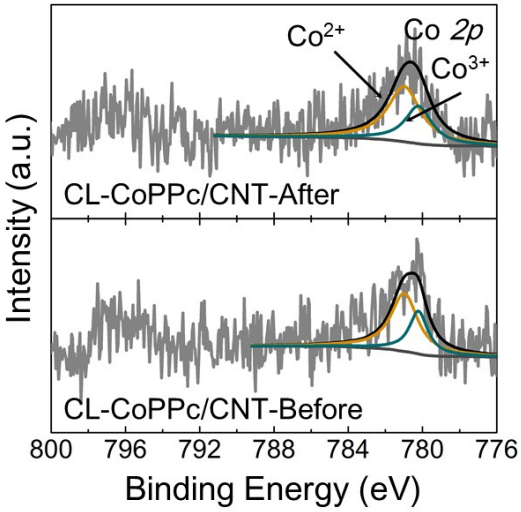

Figure S18. The high-resolution XPS spectra of Co 2*p* for CL-CoPPc/CNT before (bottom) and after (top) reaction.

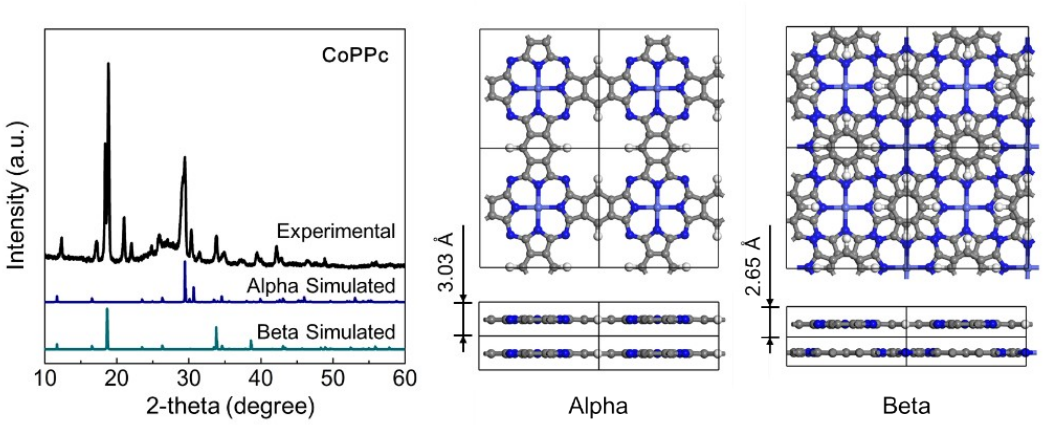

Figure S19. XRD patterns and simulation results of CoPPc.

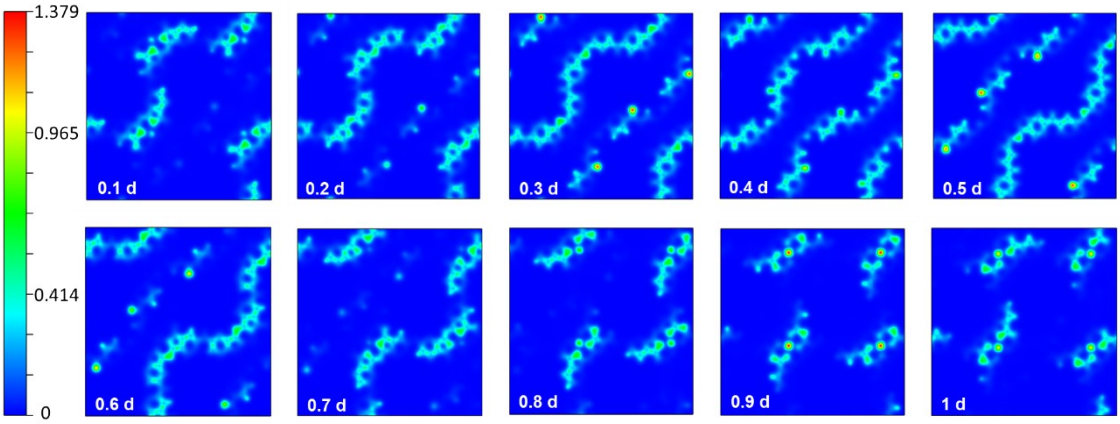

Figure S20. Electron localization functions of CL-CoPPc

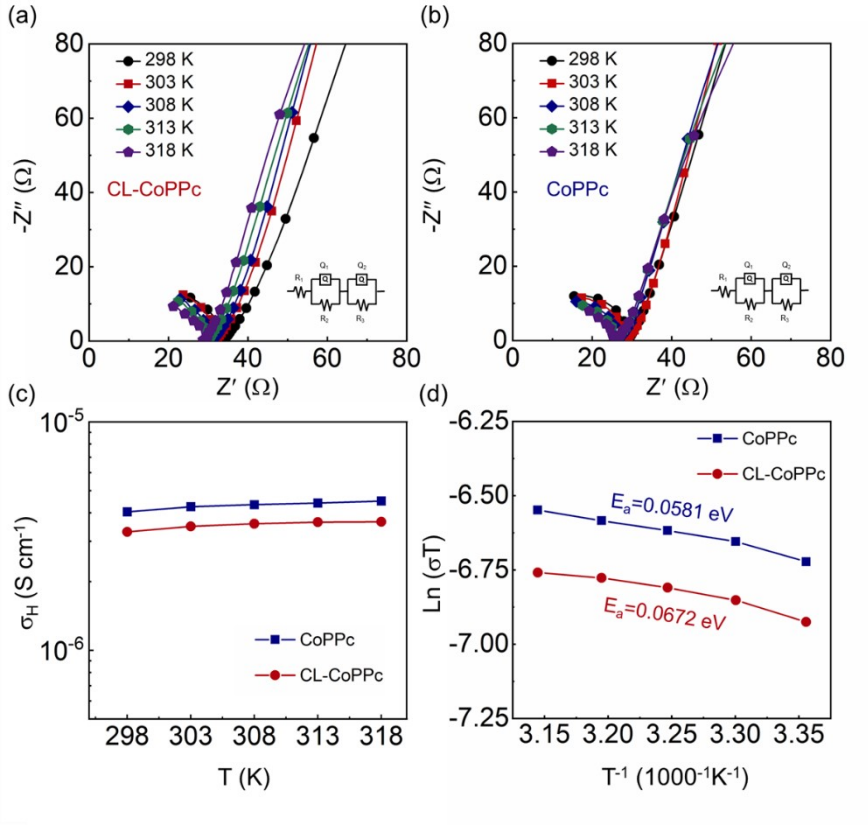

Figure. S21 Electrochemical impedance spectra of a) CL-CoPPc, b) CoPPc. c) Proton conductivity of CL-CoPPc and CoPPc at different temperatures. d) Energy barrier of CL-CoPPc and CoPPc.

We conducted electrochemical impedance spectra to measure the rate of proton transfer, and the calculated proton transfer rate of CL-CoPPc and CoPPc were 3.30×10^{-6} and 4.04×10^{-6} S cm^{-1} at 25 °C, respectively. According to the Arrhenius behavior related to proton conductivity at different temperatures, it was found that CL-CoPPc showed a higher energy barrier (0.067 eV) than that of CoPPc (0.058 eV), which also indicated the rate of proton transfer on CL-CoPPc was slower than CoPPc.

Table S1. The Co-, O-, N- and C-content of CoPc, CoPPc and CL-CoPPc. The capacitance of two Co moieties, two N moieties and three O moieties of the above three samples.

Sample	Surface chemistry (XPS)			
	Co (at%)	O (at%)	N (at%)	C (at%)
CoPc	2.56	1.93	39.22	56.29
CoPPc	0.41	4.84	8.79	85.96
CL-CoPPc	0.73	18.14	10.95	70.17
Sample	Functionality (% of total Co 2p)			
	Co (II)		Co (III)	
CoPc	69.6		21.1	
CoPPc	62.7		28.2	
CL-CoPPc	55.6		44.4	
Sample	Functionality (% of total N 1s)			
	Metal-N		N-C	
CoPc	6.8		93.2	
CoPPc	52.0		48.0	
CL-CoPPc	67.9		32.1	
Sample	Functionality (% of total O 1s)			
	O-H	O-C	O=C	
CoPc	25.4	54.3	20.3	
CoPPc	47.6	46.5	5.9	
CL-CoPPc	2.1	4.8	93.1	

Table S2 Electrical conductivity of CL-CoPPc, CoPPc and CoPc

	Conductivity (S cm^{-1})
CL-CoPPc	7.07×10^{-6}
CoPPc	7.19×10^{-5}
CoPc	2.84×10^{-7}
CL-CoPPc with CNT	21.28
CoPPc with CNT	23.56
CoPc with CNT	25.54

Table S3. Summary of the CO_2RR performances on representative high-performance electrocatalysts under diverse conditions.

Catalyst	Electrolyte	Current Density	Faradaic Efficiency	TOF	Ref.
CL-CoPPc/CNT	0.5 M $KHCO_3$	50 mA cm^{-2} @ η = 540 mV	90% @ η = 540 mV	11898 hr^{-1} @η = 0.54 V	This work
CoPPc/CNT	0.5 M $KHCO_3$	18.7 mA cm^{-2} @ η = 0.5 V	>80% @ η = 0.34 V	>4800 h^{-1} @ η = 0.5 V	[2]
D-P-CoPc	0.5 M $KHCO_3$	2.45 mA cm^{-2} @ η = 0.49 V	~ 97 % @ η = 0.49 V	412 h^{-1} @ η = 0.49 V	[3]
CoPc-2H2Por COF	0.5 M $KHCO_3$	8.1 mA cm^{-2} @ η = 0.44 V	95 % @ η = 0.44 V	~320 h^{-1} @ η = 0.44 V	[4]
Fe^{3+}-N-C	0.5 M $KHCO_3$	~50 mA cm^{-2} @ η = 0.3 V	~90% @ η = 0.3 V	N.A.	[5]
Sn/Cu-PVDF	0.1 M $KHCO_3$	~100 mA cm^{-2} @ η = 1.09 V	~80% @ η = 1.09 V	N.A.	[6]
V-CuInSe2	0.5 M $KHCO_3$	112 mA cm^{-2} @ η = 0.59 V	91% @ η = 0.59 V	N.A.	[7]
NiPc-OMe-MDE	1 M $KHCO_3$	150 mA cm^{-2} @ η = 0.5 V	99.6% @ η = 0.5 V	12 s^{-1} @ η = 0.5 V	[8]
CoPc-CN/CNT	0.1 M $KHCO_3$	15 mA cm^{-2} @ η = 0.52 V	98% @ η = 0.52 V	4.1 s^{-1} @ η = 0.52 V	[9]
CoPc2/CNT	0.5 M $NaHCO_3$	70.5 mA cm^{-2} @ η = 0.54 V	94% @ η = 0.54 V	1.67 s^{-1} @ η = 0.54 V	[10]
MOF-1992	0.1 M $KHCO_3$	16.5 mA cm^{-2} @ η = 0.52 V	80% @ η = 0.52 V	720 h^{-1} @ η = 0.52 V	[11]
CuPPc@CNT	0.1M $CsHCO_3$	6.9 mA cm^{-2} @ η = 0.59 V	80% @ η = 0.59 V	N.A.	[12]
D-CoPPc-CNT	0.5 M $NaHCO_3$	8 mA cm^{-2} @ η = 0.59 V	97% @ η = 0.59 V	1400 h^{-1} @ η = 0.49 V	[13]

References

[1] O. Bertha, S. M. Park and N. Doddapaneni, *Journal of the Electrochemical Society*, 1996, **143**, 1800-1805.

[2] N. Han, Y. Wang, L. Ma, J. G. Wen, J. Li, H. C. Zheng, K. Q. Nie, X. X. Wang, F. P. Zhao, Y. F. Li, J. Fan, J. Zhong, T. P. Wu, D. J. Miller, J. Lu, S. T. Lee and Y. G. Li, *Chem*, 2017, **3**, 652-664.

[3] H. H. Wu, M. Zeng, X. Zhu, C. C. Tian, B. B. Mei, Y. Song, X. L. Du, Z. Jiang, L. He, C. G. Xia and S. Dai, *Chemelectrochem*, 2018, **5**, 2717-2721.

[4] J. J. Yuan, S. T. Chen, Y. Y. Zhang, R. J. Li, J. Zhang and T. Y. Peng, *Advanced Materials*, 2022, **34**, 2203139.

[5] J. Gu, C. S. Hsu, L. C. Bai, H. M. Chen and X. L. Hu, *Science*, 2019, **364**, 1091-1094.

[6] W. B. Ju, F. Z. Jiang, H. Ma, Z. Y. Pan, Y. B. Zhao, F. Pagani, D. Rentsch, J. Wang and C. Battaglia, *Advanced Energy Materials*, 2019, **9**,1901514

[7] J. J. Wang, X. R. Zheng, G. J. Wang, Y. H. Cao, W. L. Ding, J. F. Zhang, H. Wu, J. Ding, H. L. Hu, X. P. Han, T. Y. Ma, Y. D. Deng and W. N. Hu, *Advanced Materials*, 2022, **34**, 2106354.

[8] X. Zhang, Y. Wang, M. Gu, M. Y. Wang, Z. S. Zhang, W. Y. Pan, Z. Jiang, H. Z. Zheng, M. Lucero, H. L. Wang, G. E. Sterbinsky, Q. Ma, Y. G. Wang, Z. X. Feng, J. Li, H. J. Dai and Y. Y. Liang, *Nature Energy*, 2020, **5**, 684-692.

[9] X. Zhang, Z. S. Wu, X. Zhang, L. W. Li, Y. Y. Li, H. M. Xu, X. X. Li, X. L. Yu, Z. S. Zhang, Y. Y. Liang and H. L. Wang, *Nature Communications*, 2017, **8**, 14657.

[10] M. Wang, K. Torbensen, D. Salvatore, S. X. Ren, D. Joulié, F. Dumoulin, D. Mendoza, B. Lassalle-Kaiser, U. Isci, C. P. Berlinguette and M. Robert, *Nature Communications*, 2019, **10**, 1-8.

[11] R. Matheu, E. Gutierrez-Puebla, M. A. Monge, C. S. Diercks, J. Kang, M. S. Prévot, X. K. Pei, N. Hanikel, B. Zhang, P. D. Yang and O. M. Yaghi, *Journal of the American Chemical Society*, 2019, **141**, 17081-17085.

[12] D. Karapinar, A. Zitolo, T. N. Huan, S. Zanna, D. Taverna, L. H. G. Tizei, D. Giaume, P. Marcus, V. Mougel and M. Fontecave, *Chemsuschem*, 2020, **13**, 173-179.

[13] J. C. Chen, J. Y. Li, W. L. Liu, X. H. Ma, J. Xu, M. H. Zhu and Y. F. Han, *Green Chemistry*, 2019, **21**, 6056-6061.